Lawrence Berkeley Laboratory
UNIVERSITY OF CALIFORNIA

EARTH SCIENCES DIVISION

Presented at the 20th ASME/AIChE Heat Transfer Conference, Milwaukee, WI, August 2-5, 1981, Paper #81-HT-52; and submitted to the Journal of Geophysical Research

HEAT AND MASS TRANSFER IN A FAULT-CONTROLLED GEOTHERMAL RESERVOIR CHARGED AT CONSTANT PRESSURE

K.P. Goyal and T.N. Narasimhan

December 1981

Prepared for the U.S. Department of Energy under Contract W-7405-ENG-48

DISCLAIMER

HEAT AND MASS TRANSFER IN A FAULT-CONTROLLED GEOTHERMAL RESERVOIR CHARGED AT CONSTANT PRESSURE

K. P. Goyal and T. N. Narasimhan

Earth Sciences Division, Lawrence Berkeley Laboratory
University of California, Berkeley, California 94720

ABSTRACT

A two-dimensional mathematical model of a fault controlled geothermal reservoir has been developed. Heated lighter water, rising in the fault, is assumed to charge a reservoir which, in turn, is overlain by a thin impermeable, thermally conducting cap rock. The mass flow rate or the pressure associated with the charging process at the fault inlet is unknown and can only be estimated. Thus, in this paper, the pressure in the fault at the bottom of the reservoir is assumed to be prescribed. Quasi-analytic solutions for the velocity, pressure, and temperature are obtained in the fault-reservoir system for a high Rayleigh number flow. In this approximation, the upwelling fluid does not cool off appreciably until it reaches the cold upper boundary of the reservoir and encounters conductive heat loss. This thermal boundary layer, which is thin at the top of the fault, grows outward laterally and occupies the full thickness of the aquifer far away from the fault. The mathematical model is based on the flow of liquid water in a saturated porous medium. The solution techniques involve the combination of perturbation methods, boundary layer theory and numerical methods. The analysis of this generic model can be applied to liquid dominated geothermal systems where the thickness of the impermeable caprock is very small compared to the depth of the reservoir.

NOMENCLATURE

C_p'	specific heat of the liquid at constant pressure, $m^2/sec-K$
g'	acceleration due to gravity, m/sec^2
K'	fault permeability and horizontal permeability in the aquifer, m^2
L'	depth of the reservoir, m
M'	mass flow rate per unit length in the direction perpendicular to the plane of paper, kg/m-sec
p'	fluid pressure in the aquifer, Pascals
P'	fluid pressure in the fault, Pascals
P_b'	specified fluid pressure in the fault at $z' = -L'$, Pascals
P_H'	cold hydrostatic fluid pressure with respect to density ρ_o', Pascals
T'	fault temperature, K
T_{max}'	maximum temperature at the hot bottom boundary of the reservoir, K
T_o'	ambient temperature, K
v'	horizontal Darcy mass flux in the aquifer per unit area, kg/m^2-sec
V'	horizontal Darcy mass flux in the fault per unit area, kg/m^2-sec
W'	vertical Darcy mass flux in the fault per unit area, kg/m^2-sec
y_e'	semifault width, m
α_e'	coefficient of thermal expansion of the liquid, K^{-1}
θ'	aquifer temperature, K

λ_m' thermal conductivity of the porous medium, Kg-m/sec^3-K

ν' kinematic viscosity, m^2/sec

ρ' density of the liquid at the temperature T', kg/m^3

ρ_o' density of the liquid at the ambient temperature T_o', kg/m^3

INTRODUCTION

The analysis of available geophysical data from various geothermal systems has made it possible to develop conceptual reservoir models which contain elements of physical plausibility. Such availability has helped to evolve extremely idealized mathematical models for heat and mass transfer in unexploited liquid dominated geothermal systems in a form which is at least physically viable. The hypothetical idealized models, developed by extensions of classical hydrodynamic stability theory in porous media (see review articles by Combarnous and Bories [1], Cheng [2], Garg and Kassoy [3]) lack both the significant internal structure and boundary conditions relevant to real geothermal systems and thus preclude the comparison of theoretical prediction with field measurements. For example, the convective configuration associated with an incompletely defined system (infinite slab configuration) or simplified thermal boundary condition (uniform temperature on a horizontal boundary) may not resemble those obtained in real systems where geological structure (the combination of fracture zones, faults and aquifers), boundary irregularity and localized intrusive bodies may have a significant effect on the flow dynamics.

Hypothetical, but more plausible models, containing the elements of configurational, structural and thermal reality have developed into a variety of ways since the pipe models of Einarsson [4], Wooding [5], Elder [6] and Donaldson [7,8]. Such models have been surveyed by Goyal and Kassoy [9]. Einarsson's pipe model concept arises from the hydrodynamic imbalance that exists between the heated, low density

water in the active part of a geothermal reservoir and the colder, denser water in the peripheral region.

Attempts have been made in the literature to develop models of exploited as well as unexploited geothermal systems on the basis of known field data. Such models include Wooding's [5] crosssectional model of up-flow in the Wairakei system; the two-dimensional areal reservoir model for Wairakei by Mercer et al. [10] and Mercer and Faust [11]; Sorey's [12] large-scale vertical model of the Long Valley Caldera, The Salton Sea reservoir areal model developed by Riney et al. [13], three dimensional model of the Cerro Prieto field by Lippmann and Goyal [14], two dimensional vertical model of the Wairakei system by Pritchett et al. [15], and a vertical profile analysis of the East Mesa system by Goyal [16] and Goyal and Kassoy [17]. Geothermal hot springs were modeled by Sorey [18] as an isolated cylindrical conduit and as a fault plane conduit to determine the amount of heat lost by conduction to the rocks surrounding the spring. In these models Sorey [18] prescribed the fluid mass flux and temperature at the base of the conduit and allowed the same mass flux to be removed from its top.

In this paper we present a two-dimensional generic type model similar to that of Goyal and Kassoy [9], for a liquid dominated geothermal reservoir charged by heated water from a vertical fault zone. Earlier, Goyal and Kassoy [9] considered a constant flux boundary condition at the bottom of the fault. In this study, however, we assume a boundary condition such that the pressure in the fault at the

bottom of the reservoir is prescribed. Additionally, the analysis can also be used to compute the velocity field in response to changes in viscosity or permeability under a prescribed pressure gradient. This boundary condition is practically realistic since it is far easier to measure reservoir fluid pressures than fluid fluxes or velocities. In practice, it may possibly be difficult to exactly locate the fault and then to measure the pressure in the fault at the bottom of the reservoir. However, the bottom of the reservoir can be estimated from the well logs and the shut-in pressure measured at this depth in a well very near the fault zone can be a reasonable estimate of this prescribed pressure as shown in Goyal and Kassoy [9,17]. The governing equations pertain to heat and mass transfer in saturated permeable media. The solution technique used involves a combination of perturbation methods, boundary layer theory and numerical methods. Results are presented for pressures, velocities, temperatures and temperature gradients in the fault-aquifer system.

DEVELOPMENT OF CONCEPTUAL MODEL

Studies of liquid-dominated geothermal systems such as those at Wairakei (Grindley [19]), Broadlands (Grindley [20]), Long Valley (Rinehart and Ross [21]), Imperial Valley (Elders et al. [22]), Cerro Prieto (Puente and de la Peña [23]) and Ahuachapan (Ward and Jacobs [24]) suggest that geothermal anomalies are intimately associated with a specific pattern of faulting. For example, at East Mesa in the Imperial Valley of California, the Mesa fault is believed to act as conduit for the hot waters rising up from the depth (Combs and Hadley

been heated up in the fractured basement system. The mass flow rate or the pressure associated with the charging processes at the fault inlet cannot be known without a global analysis of the entire convection process. In the present analysis the pressure in the fault at the bottom of the reservoir is considered to be a prescribed parameter. The hot light liquid rises up in the reservoir section of the fault and is pushed into the aquifer due to the overpressure associated with the convection process. The liquid is assumed to flow only horizontally within the aquifer. The vertical permeability of the formation is expected to be drastically reduced due to the presence of interbedded shaley and sandy layers (Bailey [26]). Except for flow within vertical fractures, any net vertical flow in the reservoir will depend upon the sand continuity in the vertical direction. During East Mesa Modeling efforts, Riney et al. [27] found that the vertical reservoir permeabilities of about 0.3-0.5 md and horizontal reservoir permeabilities of about 90 md were necessary to match the observed field data.

For mathematical purposes the fracture zone is idealized as a vertical slab of homogeneous and isotropic porous material. The adjacent aquifer is represented as a porous medium of lateral half width H' with horizontal permeability much larger than the vertical value of small absolute magnitude. The impermeable upper boundary is assumed to be exposed to ambient conditions. Thus we prescribe a constant temperature boundary condition at the cold upper boundary. The temperature boundary condition at the bottom of the reservoir is derived from the temperatures measured in thirteen wells of the East

[25]). Bailey [26] hypothesized that the East Mesa geothermal reservoir owes its presence to the charging of hot waters from the fault at an intersection with an aquifer of sufficient horizontal permeability. A two dimensional model of this system is discussed in Goyal and Kassoy [17] where a thick clay cap separates the reservoir from the ground surface. In this study, we consider a similar but a simplified model which has a very thin impermeable clay cap represented by an upper cold boundary of the reservoir as shown in figure 1. Our results of this study will, therefore, be applicable to a system where the thickness of the clay cap is orders of magnitude smaller than the reservoir depth or where the heated water is present in an extensive region just below the surface. While we were motivated by observations of the East Mesa field, it is not our intention to use the model to describe East Mesa in detail. The purpose of this paper is to provide an analytical solution for a gross understanding of a geothermal system during the exploratory phase. As more subsurface data becomes available for a clearer definition of the reservoir, numerical methods will be more appropriate for detailed reservoir analysis.

The fault is considered to be a vertically oriented region, composed of highly fractured material of finite width ($2 y_e'$). It extends downward through the interbedded sediments of the reservoir for a distance L' to the basement rock. The depth of the reservoir (L') is assumed to be much larger than the fault width ($2 y_e'$). It is postulated that the fault is charged at depth by water which has

Mesa system occupying an area of about six square miles. As shown in Fig. 2, the temperatures in these wells converage to a value of about 200°C at the depth of about 2.5-3 km. This motivated us to prescribe a constant temperature boundary condition at the bottom of the reservoir. At the vertical boundary far from the fault ($H' >> L' >> y'_e$) the temperature distribution is assumed to be controlled by vertical conduction, the pressure distribution is hydrostatic, and mass flux entering the fault zone is allowed to leave the aquifer from its far field boundary at $y' = H'$.

It is to be emphasized that this model is only a part of a "global circulation pattern." It does not define the downflow and heat up zones, and thus input mass or the pressures at the bottom of the fault are unknown. The driving mechanism for the convection, the result of a hydrostatic pressure imbalance between the hot upflow region and the cold downflow region, is identical to that envisioned by Donaldson [7].

MATHEMATICAL MODEL

A detailed derivation of the governing equations for a thermally active, saturated, deformable porous material is given by Goyal [16]. The equations used in the present study are obtained from the above by assuming that the flow is steady, the solid matrix is rigid, the fault medium is homogeneous and isotropic, liquid properties are constant, the thermal conductivities of the fault and aquifer media are constant and equal, and that the vertical permeability in the aquifer is much smaller than the horizontal value. Thus for all practical purposes vertical

velocity in the aquifer is nearly zero. We also assume that the horizontal permeability in the reservoir is equal to that of the fault for mathematical simplicity and may not be true in actual field situations. However, Goyal and Kassoy [17] modeled East Mesa system under a similar assumption and the predicted results matched favorably with those measured in the field. Riney and Pritchett [28] studied the effect of introduction of a fault model on the subsurface isotherms and the surface heat flow patterns in the East Mesa field, using a similar assumption. In addition, the Boussinesq approximation is invoked. The dimensional equations for the system shown in Fig. 1 and the related boundary and continuity conditions are given in the Appendix.

Within the fault, where the characteristic horizontal dimension and velocity component are much smaller than their vertical counterparts, appropriate nondimensional variables can be defined as:

$$\bar{y} = y'/y'_e \quad , \quad y_e = y'_e/L' \quad , \quad z = z'/L'$$

$$\bar{V} = V'/y_e q'_o \rho'_o \quad , \quad W = W'/q'_o \rho'_o \quad , \quad T = T'/T'_o \quad , \qquad (1)$$

$$\tau = (T'_{max} - T'_o)/T'_o \quad , \quad P = (P' - P'_H)/p'_o \quad ,$$

where τ is defined as the overheat ratio. Symbols with prime indicate a dimensional quantity while those without it a nondimensional quantity. The horizontal velocity in the fault is smaller than its vertical counterpart because the area perpendicular to flow in y-direction is $(1/y_e)$ times that in z-direction. Substitution of Eq. (1) into Eqs. (A1)

to (A5) leads to an inherent balance between the buoyancy, Darcy, and pressure terms in the vertical momentum equation, if

$$q_o' = \frac{\alpha_e' \Delta T' g' K'}{\nu'} = \text{reference convection velocity}$$

$$p_o' = \rho_o' g' \alpha_e' L' \Delta T' = \text{reference convection pressure} \qquad (2)$$

$$R = \frac{\rho_o' q_o' C_p' \Delta T'}{\lambda_m' (\Delta T'/L')} = \text{Rayleigh number}$$

where $\Delta T' = T_{max}' - T_o'$. The nondimensional equations, transformed boundary and continuity conditions relevant in the fault zone obtained by using Eqs. (1) and (2) in Eqs. (A1)-(A3), (A6), (A7) and (A10b) can be written as

Fault Zone:

$$\bar{V}_{\bar{y}} + W_z = 0 \quad ; \quad y_e^2 \bar{V} = -P_{\bar{y}} \quad ; \quad W = -P_z + (T-1)/\tau \qquad (3a\text{-}c)$$

$$\gamma^2 (\bar{V} T_{\bar{y}} + W T_z) = T_{\bar{y}\bar{y}} + y_e^2 T_{zz} \quad ; \quad \gamma = R^{1/2} y_e \qquad (4a,b)$$

$$W(\bar{y},0) = 0 \quad ; \quad P(\bar{y},-1) = P_b \quad ; \quad P_b = (P_b' - P_H')/p_o' \qquad (5a\text{-}c)$$

$$T(\bar{y},0) = 1 \quad ; \quad T(\bar{y},-1) = 1 + \tau \quad ; \quad T_{\bar{y}}(0,z) = 0 \quad ; \quad \bar{V}(\pm 1,z) = \pm v(z) \qquad (6a\text{-}d)$$

For the aquifer, within which the horizontal scale is measured by $\hat{y} = y'/H'$, the pressure $p = P$, the temperature $\theta = T$, and the velocity $v = \bar{V}$, the appropriate system of equations obtained from Eqs. (A4) and (A5) is given by:

Aquifer:

$$v(z) = -p_{\hat{y}}/d \quad ; \quad d\gamma^2 v(z)\, \theta_{\hat{y}} = y_e^2 \theta_{\hat{y}\hat{y}} + d^2 \theta_{zz} \tag{7a,b}$$

where

$$H'/L' = d/y_e \quad , \quad d = O(1) \text{ number} \tag{8a,b}$$

The magnitude of H' with respect to the fault depth, L', given in Eq. (8a) is chosen to ensure a balance between the nondimensional aquifer velocity v and the horizontal pressure gradient as shown in Eq. (7a). The number d, used in this study to define the location of the far field boundary (y' = H') of the aquifer, will be determined during the course of this paper. It is assumed that the hot liquid loses its heat to the surroundings to the extent that the horizontal temperature gradient becomes vanishingly small far from the fault. It may be emphasized that horizontal motion exists at the far field boundary (y' = H') but that heat transfer is due to vertical conduction only. The related boundary conditions as obtained from Eqs. (A8), (A10a) and (A9) are:

$$\theta(\hat{y},0) = 1 \quad ; \quad \theta(\hat{y},-1) = 1 + \tau \tag{9a,b}$$

$$\theta(\hat{y} = y_e^2/d, z) = T(\bar{y} = 1, z) \quad ; \quad \theta(\hat{y}=1, z)\ 1 - \tau z \tag{10a,b}$$

The parameter γ is assumed to be an O(1) number because y_e is considered small. If, for instance, we consider $R = 10^3$ and L' = 2 km then $y_e' = 63.2\ \gamma$ meters, indicating that reasonable fault zone thicknesses can be incorporated in the theory. In the mathematical

analysis solutions are sought in the limit of large R with $\gamma = O(1)$ implying, of course that y_e is small.

Large values of R suggest that energy transfer associated with liquid convection is far greater than that due to conduction. In this regard one may expect that fluid particles moving through the system will tend to behave isothermally unless affected by cooling associated with a relatively cold boundary.

The cooling effect of the surface is confined to a thin thermal boundary layer near the top of the fault for a high Rayleigh number flow. The boundary layer grows as the fluid moves away from the fault and virtually occupies the whole depth of the aquifer far away from fault. Thus, the flow outside the boundary layer is an isothermal flow.

It can be noted from Eq. (3b) that the horizontal pressure gradient in the fault is very small, $O(y_e^2)$. Thus, the basic fault pressure is only a function of depth and can be calculated in terms of W and v. The horizontal aquifer velocity v(z) can then be calculated explicitly from Eq. (7a) because the far field ($y' = H'$) pressure is known, once Eq. (10b) is specified. Upon decoupling the fluid mechanics from the thermal problem, the energy Eq. (7b) can then be solved for the temperatures in the aquifer.

CLOSED FORM SOLUTIONS IN THE FAULT AQUIFER SYSTEM

The water in the fault zone rises up adiabatically because the convection Rayleigh number is considered to be large. Even the liquid

in the aquifer just adjacent to the fault remains at the supply temperature. Cooling in the fault itself can take place only in a thin boundary layer just below the cold upper surface. The uppermost portion of the neighboring aquifer is similarly affected.

The basic solutions in the isothermal portions of the fault and aquifer system are (Goyal and Narasimhan [29]):

$$T = 1 + \tau \tag{11}$$

$$\bar{V} = \bar{y}\left[\frac{C_1}{d}\cosh z/\sqrt{d} + b_1 \sinh z/\sqrt{d} - 1\right] + O(y_e^2) \tag{12}$$

$$W = -\frac{C_1}{\sqrt{d}}\sinh z/\sqrt{d} - \cosh z/\sqrt{d} + z + 1 + O(y_e^2) \tag{13}$$

$$P = d\left\{\frac{C_1}{d}\cosh z/\sqrt{d} + b_1 \sinh z/\sqrt{d} - 1\right\} - z^2/2 + O(y_e^2) \tag{14}$$

$$v(z) = \frac{C_1}{d}\cosh z/\sqrt{d} + b_1 \sinh z/\sqrt{d} - 1 + O(y_e^2) \tag{15}$$

$$p = v(z)\, d(1 - \hat{y}) - z^2/2 + O(y_e^2) \tag{16}$$

where

$$C_1 = \frac{P_b + d + \frac{1}{2} + \sqrt{d}\sinh\frac{1}{\sqrt{d}}}{\cosh\frac{1}{\sqrt{d}}} \quad , \quad b_1 = \frac{1}{\sqrt{d}} \tag{17a,b}$$

It can be noted that $(-z^2/2)$ is the pressure at the far field boundary ($y' = H'$) of the aquifer and is consistent with the specified temperature field (Eq. (10b)). The solutions for the vertical velocity (W) and overpressure (P) in the fault, as given by Eqs. (13) and (14) respectively are obtained for a prescribed pressure P_b' at $Z' = -L'$. It is now possible to calculate mass flux entering the fault at $z' = -L'$ from Eq. (13) and Eq. (1). This suggests that mass flux and pressure at $z' = -L'$ are uniquely related. The exact form of their relationship is discussed in Fig. 11.

BOUNDARY LAYER SOLUTIONS

According to Eq. (6a), the nondimensional temperature at the top of the fault is 1. There should be a boundary layer to accommodate the temperature drop from $1 + \tau$ to 1. Using the appropriately scaled variables

$$\bar{z} = z/y_e \quad \text{and} \quad \bar{W} = W/y_e \tag{18a,b}$$

boundary layer solutions in the fault, as discussed in Goyal and Narasimhan [29] are

$$\bar{V} = \left(\frac{C_1}{d} - 1\right)\bar{y} + O(y_e) \quad , \quad \bar{W} = -\left(\frac{C_1}{d} - 1\right)\bar{z} + O(y_e) \tag{19a,b}$$

$$T = 1 - \tau\ \mathrm{erf}(A\bar{z}) + O(y_e) \tag{20}$$

$$P = d\left[\frac{C_1}{d} - 1\right] - y_e\left\{\bar{z}\ \mathrm{erf}(A\bar{z}) + \frac{1}{A\sqrt{\pi}}\ e^{-A^2\bar{z}^2}\right\} + O(y_e^2) \tag{21}$$

where

$$A = \sqrt{\gamma^2\left(\frac{C_1}{d} - 1\right)}\Big/2 \tag{22}$$

The thermal boundary layer initiated at the top of the fault continues into the adjacent aquifer over a horizontal distance of scale y_e'. In this initial aquifer zone of water cooling, the solutions for velocity and overpressure are:

$$v(\bar{z}) = \left(\frac{C_1}{d} - 1\right) + O(y_e) \quad ; \quad p(\hat{y},\bar{z}) = d\left(\frac{C_1}{d} - 1\right)(1 - \hat{y}) + O(y_e) \tag{23a,b}$$

TEMPERATURE DISTRIBUTIONS WITHIN THE AQUIFER

Once the velocity field in the aquifer is known the temperature can be calculated from the energy equation. This must be done for five different regions shown in Fig. 3. To obtain temperatures in the near fault regions where length scale is of $O(y_e')$ and $O(L')$ the aquifer energy equation (Eq. (7b)) is transformed for these length scales as discussed in Goyal and Narasimhan [29] and Goyal and Kassoy [9]. The solution in region 1 can be written as

$$\theta(\bar{y},\bar{z}) = 1 - \frac{2_\tau}{\pi}\int_\infty^0 \exp\left\{-\frac{\omega^2}{4A^2} - A^2 + \sqrt{A^4 + \omega^2}\right.$$
$$\left. + (A^2 - \sqrt{A^4 + \omega^2})\,\bar{y}\right\}\frac{\sin\,\omega\bar{z}}{\omega}\,d\omega \tag{24}$$

A similarity solution, compatible with the solution in region 1 can be obtained in the region 3. Elementary methods yield

$$\theta(y,z^*) = 1 - \tau \operatorname{erf}\left(\frac{A}{\sqrt{2}}\,\eta\right), \quad \eta = z^*/y^{1/2}, \quad y = \frac{y'}{L'}, \quad z^* = \frac{z}{ye^{1/2}} \tag{25a-d}$$

It is possible to obtain an analytical solution of Eq. (7b) in region 5, when $\hat{y} \ll 1$ and $z \ll 1$, such that $z/\hat{y}^{1/2} = O(1)$, which can be matched with Eq. (25a). We find the form

$$\theta(\hat{y},z) = 1 - \tau \operatorname{erf}\left[\frac{A}{\sqrt{2d}}\,\frac{z}{\hat{y}^{1/2}}\right] + \frac{\hat{y}^{1/2}\,\tau\gamma^2}{4\sqrt{2d}\,A^2}\left[\frac{z}{\sqrt{2d\hat{y}}}\left\{1 + \operatorname{erf}\left(\frac{Az}{\sqrt{2d\hat{y}}}\right)\right\} - \frac{Az^2}{d\hat{y}\sqrt{\pi}}\,e^{-\frac{A^2z^2}{2d\hat{y}}}\right] + O(\hat{y}) \tag{26}$$

by using coordinate expansion methods. This solution provides the transition between the incompatible conditions $\theta(\hat{y},0) = 1$, $\theta(\hat{y}\geq 0,z) = 1 + \tau$ for $|z| > 0$ in the vicinity of the singular corner $\hat{y} = z = 0$.

The energy equation in Eq. (7b), parabolic to the lowest order, must be solved subject to the boundary conditions in Eqs. (9a) and (9b) and the initial condition $\theta(\hat{y}\geq 0,z) = 1 + \tau$ for $|z| > 0$ obtained from matching with region 4. The last formal condition at the far end of the aquifer, Eq. (10b), is used to determine a value for d. Numerical integration by standard finite difference methods is carried out for assumed values of d until the solution at the far edge ($y' = H'$) is within 0.5 percent of the real condition. This approximation provides an engineering-type estimate of the boundary location. At that point

convection of energy associated with the $\theta_{\hat{y}}$-term in Eq. (7b) is very small compared to the conduction term. Of course in the formal mathematical sense, the purely conductive profile can be found only for $\hat{y} \to \infty$. From the mathematical viewpoint, the reduction of the full-elliptic problem in region 1 to the parabolic system in region 5 of the aquifer permits a simplified numerical computation procedure. The fact that the reduction can be developed in a formal, rational manner for the large Rayleigh number approximation shows that the imposition of the boundary condition at an a priori specified location ($y' = H'$) is fundamentally unsound. In physical terms, this implies that the thermal anomaly associated with the upward fault zone flow has a natural horizontal relaxation length, associated basically with the distance required to transfer out of the surface, heat in excess of that arising from the natural geothermal gradient $\Delta T'/L'$. A quantitative indication of this matter involves the evaluation of d.

RESULTS AND DISCUSSION

It is imperative that the analysis carried out in the preceding sections should be applied for the parameters which are representative of a typical geothermal system. Consider a geothermal system with following typical data.

$y_e' = 75$ m

$L' = 3000$ m

$T_o' = 298$ K

$\Delta T' = 298$ K

$K = 10^{-13}$ m^2

$\lambda_m' = 2.125$ W/m-k (Goyal and Kassoy [17])

Using the physical properties of water at 298 K, the following reference values can be calculated.

$q_0' = 8.5 \times 10^{-8}$ m/s

$p_0' = 22.74 \times 10^5$ Pa .

The corresponding nondimensional numbers as given below are selected in our calculations.

$R = 500$, $\tau = 1$, $y_e = 0.025$

For a selected set of nondimensional numbers, R, τ, y_e and P_b, as shown in Table 1, Eq. (7b) is integrated to obtain an value of d, representative of that set. It can be seen that d is different for different sets of parameters. It may be observed from this table that an increase in P_b, R, or y_e increases d; which means that a larger aquifer is needed for the transition to the conduction temperature profile when the parameter is increased. In physical terms this result implies that the hot isothermal portions of the aquifer, maintained by horizontal convection effects will be more extensive in systems of relatively larger fault inlet pressure, permeability and fault size.

The dependence of various parameters on the velocity, pressure, temperature and surface heat flux in the fault and the aquifer is given in Figs. 4 to 10. The value of d used in these figures is for the parameters shown.

Figure 4 shows the vertical velocity (W) in the fault as obtained from Eq. (13) at various depths for different inlet pressures (P_b). It may be noted that an increase in the inlet pressure leads to an

increase in the vertical velocity. It is consistent with the commonly held notion that one would require higher pressure to push more mass into the system. The vertical velocity vanishes at the top of the fault due to the impermeable boundary assumption. All the water is pushed to the aquifer by the time it reaches the top surface of the fault. Dimensional vertical velocity (W') in the fault can be obtained by multiplying W of Fig. 4 by $\rho_o' q_o'$. The nondimensional ordinate (z) can be converted into dimensional depth by multiplying it by the depth of the reservoir (L'). The dimensional specified pressure P_b' can be obtained by adding hydrostatic pressure P_H' to the product of P_b and reference convection pressure p_o'.

Figure 5 is a plot of fault overpressure (P) versus depth for different values of P_b as computed from Eq. (14). As one may expect, the overall fault pressures increase for an increased inlet pressure (P_b). It may be noted that the fault pressures decrease upwards and then increase toward the top of the fault. This increase toward the top is caused by the stagnation point at z = 0. The dimensional overpressure can be obtained by multiplying P_b by reference convection pressure p_o'.

The horizontal velocity in the aquifer calculated from Eq. (15) at various depths is shown in Fig. 6 for different inlet pressures. As expected, horizontal aquifer velocities increase for an increased inlet pressure. The trend of the curves is similar to the overpressure curves in Fig. 5. The larger velocities at the top of the aquifer are associated with the relatively higher horizontal pressure gradients

there. The dimensional velocity in the aquifer can be obtained by multiplying nondimensional velocities by ye $\rho_o' q_o'$.

The boundary layer temperatures in the fault are shown in Fig. 7 for various values of P_b as obtained from Eq. (20). It may be noted that only 12 percent of the total depth of the fault is shown in this figure. Higher vertical velocities associated with increased P_b give rise to higher temperatures as indicated in the figure. The thickness of the boundary layer changes from about 10 percent to about 8 percent of the fault depth for an increase in P_b from 0.5 to 2.0 respectively. Temperatures in lower 90 percent of the fault are constant and equal to the highest temperature value of $1 + \tau$. In dimensional terms P_b equal to 0.5, 1.0 and 2.0 represents about 305 bars, 316 bars and 339 bars respectively.

The fluid temperatures in the near fault regions (1 and 3) of the aquifer are shown in Fig. 8 at different horizontal locations in the reservoir. Boundary layer temperatures in region 1, and in region 3 obtained from quadrature solution (Eq. (24)) and similarity solution (Eq. (25a)) respectively are explicitly shown in this figure. As expected the quadrature solution matches the similarity solution for large values of $\bar{y}$ (y/y_e). It may be noted that the boundary layer temperatures decrease with increasing distance from the fault. This drop in temperatures is caused due to heat loss to the surroundings through the cold upper boundary. The temperatures in the lower portions of the aquifer (regions 2 and 4) are constant and equal to the highest temperature value of $1 + \tau$. The fluid temperature in

these regions remains at the supply temperature since heat loss is only confined to boundary layer regions 1 and 3. Thus a hypothetical well drilled in regions 2 and 4 should encounter a zero vertical temperature gradient regime associated purely with a horizontal flow. In contrast, conventional wisdom suggests that the observation of small vertical temperature gradients implies vigorous vertical convection. It is true, on theoretical grounds, that the latter process will generate nearly isothermal regimes, it should be clear that specific geologic structure can have a similar influence.

Figure 9 shows the variations of the aquifer temperature with depth at several locations away from the fault. The $\hat{y} = 1$ represents the far end of the aquifer, which is located at d/y_e times its depth. The temperature decrease with increasing distance from the fault can be seen in the aquifer which is affected by heat loss to the cold upper boundary. It may be noted that at $\hat{y} = 0.1$, half of the aquifer is at least within 80 percent of the high temperature value.

We shall now qualitatively validate the model profiles (Figs. 8 and 9) with a field example from East Mesa, California (Fig. 2).

The geothermal reservoir in East Mesa lies at a depth of about 800 meters from the ground surface (Goyal and Kassoy [17]). The downhole temperatures measured in various wells tapping the permeable zones are shown in Fig. 2. The temperatures measured in conduction dominated upper 800 meters are not shown in this figure, while Figs. 8 and 9 show the ambient temperature at the upper boundary of the reservoir as prescribed. For a proper comparison, it is desirable to

include the clay cap in the model being studied. In that case, large temperature gradients at the upper boundary of the reservoir ($z = 0$) caused by prescribed ambient temperature boundary conditions, will disappear as discussed in Goyal and Kassoy [17]. However, the heat transfer mechanism in the model being studied and that shown in Fig. 2 is similar if we replace the upper boundary of our model by an interface between the reservoir and the Clay Cap where the temperature will be much higher than the ambient temperature and will decrease with the distance away from the fault due to heat loss to the surface through the Clay Cap. Thus a qualitative comparison is only possible between Figs. 2, 8 and 9. It can be seen that wells 6-1, 6-2, 8-1, 44-7 and 48-7 are located in the hottest portions of the reservoir. A qualitative comparison of the borehole temperature variations in Fig. 2 and theoretical predictions in Figs. 8 and 9 shows that the temperature profiles in wells 6-1, 6-2, 8-1, 44-7 and 48-7 are similar to those in Fig. 8 pertaining to the near fault regions. This suggests that the aforementioned wells are at least close to the hot recharge zones of this field. In fact, flat temperature profiles similar to those in Fig. 8 can be seen in wells 8-1, 44-7 and 48-7 between depths of 1200-1800 meters, 1500-1850 meters and 1800-2100 meters respectively. The temperature profiles of the other wells in Fig. 2 are similar to those in Fig. 9 for $\hat{y} > 0.4$. These wells are thought to be farther away from the intensely fractured zone of the reservoir system. In particular, well 18-28 is farthest from any known fault zone.

Comparison of Figs. 8, 9 and 2 shows that the model predictions are credible at least in a qualitative sense.

Figure 10 shows the effect of fault inlet pressure on the surface temperature gradients both for the fault and the aquifer. Heat transfer at the surface increases with increasing P_b, as expected. Nondimensional pressures $P_b = 1$ and 2 represent about 316 bars and 339 bars when translated into dimensional pressures. Thus an increase of 7 percent in the dimensional fault inlet pressure increases surface heat flux by a maximum amount of about 11 percent. Matching of the three regions is shown for $P_b = 1$. It can be noted that the length of the aquifer is different for each P_b. This difference is due to different value of d associated with a different fault inlet pressure. It is found that an increase in R and y_e enhances the temperature gradients at the surface, as expected. The results imply that the fault zone convection process enhances the surface heat flux by factor of about 30 above the background conductive value.

This value is the right order of magnitude for geothermal systems with vigorous surface manifestations where heated water is present in an extensive region just below the surface. It is rather large for systems exemplified by East Mesa, Imperial Valley, California where the reservoir is separated from the surface by an extensive region of clay rich sediments. For East Mesa, the heat flux near the fracture zone is about three to four times the background value (Goyal and Kassoy [17]).

As discussed earlier in the paper, the prescribed boundary conditions M and P_b are uniquely related by the parameter d which in turn is obtained by integrating parabolic Eq. (7b) numerically until the specified boundary condition (Eq. (10b)) is satisfied.

Figure 11 shows the effect of prescribed boundary conditions M and P_b on the length of the aquifer d. M, the nondimensional mass input to the fault, is the ratio of M' and reference mass flow rate M_o' ($=2\, y_e' \rho_o' q_o'$) as defined in Goyal and Kassoy [9]. An increase in M increases d significantly more than a corresponding increase in P_b. It may be noted in this figure that a change in P_b from 1 to 2 is equivalent to an increase in M from 2.65 to 3.55 or a 100 percent increase in the prescribed nondimensional inlet pressure results only into 30 percent increase in the nondimensional input mass to the system. It suggests that the enlargement of the isothermal region in the aquifer is stronger when the input mass is doubled compared to that when inlet pressure is doubled. The detailed discussion related to the effect of various parameters listed in Table 1 on the pressures, velocities, temperatures and temperature gradients in the fault-aquifer system is given in Goyal and Narasimhan [29].

CONCLUSIONS

Quasi-analytic solutions are obtained for velocities, pressures, temperatures and temperature gradients in a fault-controlled liquid dominated geothermal system with a specified pressure at the fault inlet. The solution techniques involve the combination of perturbation

methods, boundary layer theory and numerical methods. Effect of various parameters such as fault inlet pressure, Rayleigh number, overheat ratio and fault width is investigated on these solutions. Additional results for other parameter values can be found in Goyal and Narasimhan [29].

The analysis can be applied to compute the velocity field in an aquifer in response to changes in its permeability or fluid viscosity under a prescribed inlet pressure. Also, if the geological, geophysical, heat flux and borehole logging data is known, it is possible to calculate total fluid recharge rate to the geothermal system in addition to other physical parameters of interest.

It is shown that nearly zero gradient temperature profiles in the near fault regions 2 and 4 can be associated with purely horizontal water motion (Darcy flow rate of about 2×10^{-8} m/s near the hypothesized fault) rather than only with the more vigorous upflow itself. While it is clear on theoretical grounds that the latter process will generate nearly isothermal regimes, it should be clear that specific geologic structure can have a similar effect. Thus it is reasonable to speculate that deep, high temperature, isothermal zones are at least near to the source of a geothermal system.

The concepts used to generate the model can be tested directly by comparison of the field data and the theoretical prediction. Current measurement techniques provide surface heat flux distributions, downhole temperature and pressure distributions which can be compared with values obtained in a given model. The temperatures predicted by this

model compare favorably in a qualitative sense to those measured in the East Mesa anomaly.

ACKNOWLEDGMENT

Authors would like to thank David Kassoy of the University of Colorado, Boulder, Jack Howard and Karsten Pruess of LBL for very constructive criticism.

This work was supported by the Assistant Secretary for Resource Applications, Office of Industrial and Utility Applications and Operations, Division of Geothermal Energy, of the U. S. Department of Energy under Contract W-7405-ENG-48.

APPENDIX

The dimensional equations describing the conservation of mass, momentum and energy in a fault-aquifer system, as obtained from Goyal [16] can be written as

Fault zone:

$$V'_{y'} + W'_{z'} = 0 \tag{A1}$$

$$V' = -\frac{K'}{\nu'} P'_{y'} \quad , \quad W' = \frac{K'}{\nu'}\left\{-(P' - p'_H)_{z'} + g'\rho'_o\alpha'_e(T' - T'_o)\right\} \tag{A2a,b}$$

$$C'_p\left[V'T'_{y'} + W'T'_{z'}\right] = \lambda'_m\left\{T'_{y'y'} + T'_{z'z'}\right\} \tag{A3}$$

Aquifer:

$$v'(z') = -\frac{K'}{\nu'} p'_{y'} \tag{A4}$$

$$C'_p v'\theta'_{y'} = \lambda'_m(\theta'_{y'y'} + \theta'_{z'z'}) \tag{A5}$$

The solution of the above system is subjected to the following boundary and continuity conditions.

Boundary conditions:

Fault zone:

$$W'(y',0) = 0 \quad , \quad P'(y',-L') = P'_b \tag{A6a,b}$$

$$T'(y',0) = T'_o \quad , \quad T'(y',-L') = T'_{max} \quad , \quad T'_{y'}(0,z') = 0 \tag{A7a-c}$$

Which describe an impermeable upper boundary, fault pressure at the bottom of the reservoir, the cold upper boundary, the hot lower boundary and system symmetry respectively.

Aquifer:

$$\theta'(y',0) = T_o' \quad , \quad \theta'(y',-L') = T_{max}' \quad , \tag{A8a,b}$$

$$\theta'(H',z') = T_o' - (T_{max}' - T_o') \frac{z'}{L'} \tag{A9}$$

which describe the temperatures at the cold upper boundary, the hot lower boundary and at the far field boundary of the aquifer. Equation (A9) is a formal statement of the required conduction-controlled heat transfer at the aquifer edge.

Continuity conditions at the fault-aquifer boundary:

$$T'(y_e',z') = \theta'(y_e',z') \quad , \quad V'(\pm y_e',z') = \pm v'(z') \tag{A10a,b}$$

$$P'(y_e',z') = p'(y_e',z') \tag{A11}$$

which describe the continuity of temperature, velocity and pressure respectively.

The system of Eqs. (A1) to (A11) is first nondimensionalized and then solved as discussed in the text of the paper.

REFERENCES

1. Combarnous, M. A. and S. A. Bories. Hydrothermal Convection in Porous Media. Advances in Hydrosciences, 10, 232-307, 1975.

2. Cheng, P., "Heat Transfer in Geothermal Systems," in Advances in Heat Transfer, 14 (ed. T. F. Irvine, Jr. and J. P. Hartnett), Academic Press, NY, 1-105, 1978.

3. Garg, S. K. and D. R. Kassoy. Convective Heat and Mass Transfer in Hydrothermal Systems, Geothermal Resources (eds. L. Ryback and P. Muffler), Johy Wiley and Sons, Ltd., London, 1979.

4. Einarsson, T., The Nature of the Springs of Iceland (in German), Rit, Visind. Esl. 26, 1, 1942.

5. Wooding, R. A., Steady State Free Thermal Convection of Liquid in a Saturated Permeable Medium, J. Fluid Mechanics, 2, 273-285, 1957.

6. Elder, J. W., Heat and Mass Transfer in the Earth's Hydrothermal Systems, New Zealand D. S. I. R. Bulletin #169, 1966.

7. Donaldson, I. G., A Possible Model for Hydrothermal Systems and Methods of Studying Such a Model. Third Australian Conference on Hydraulics and Fluid Mechanics, Inst. of Eng. Aust. and Univ. of N. S. W., Sidney, 202-204, 1968.

8. Donaldson, I. G., The Simulation of Geothermal Systems with a Simple Convection Model. Geothermics, special issue 2, 649-654, 1970.

9. Goyal, K. P. and D. R. Kassoy, "Fault Zone Controlled Charging of a Liquid-Dominated Geothermal Reservoir," J. Geophysical Res., vol. 85, No. B4, 1867-1875, April 1980.

10. Mercer, J. W., C. F. Pinder, and I. G. Donaldson. A Galerkin-Finite Element Analysis of the Hydrothermal System at Wairakei, New Zealand. J. of Geophysical Research, 80(17), 2608-2621, 1975.

11. Mercer, J. W. and C. R. Faust, Geothermal Reservoir Simulation III: Application of Liquid and Vapor-Dominated Hydrothermal Techniques to Wairakei, New Zealand, Water Resources Research, 15(3), 653-671, 1979.

12. Sorey, M. L., A Model of the Hydrothermal System of Long Valley Caldera, California, Summaries, Second Workshop Geothermal Reservoir Engineering, Stanford, California, 324-338, 1976.

13. Riney, T. D., J. W. Pritchett, and S. K. Garg, Salton Sea Geothermal Reservoir Simulations, Proceedings, Third Workshop Geothermal Reservoir Engineering, Stanford University, Stanford, California, 178-184, 1977.

14. Lippmann, M. J. and K. P. Goyal, Numerical Modelling Studies of the Cerro Prieto Reservoir, Lawrence Berkeley Laboratory, University of California, Berkeley, LBL-9590, Cerro Prieto-14, 11, February 1980.

15. Pritchett, J. W., L. F. Rice and S. K. Garg, Reservoir Simulation Studies: Wairakei Geothermal field, New Zealand, Lawrence Berkeley Laboratory, University of California, Berkeley, LBL-11497, GREMP-11, UC-66, p. 103, 1980.

16. Goyal, K. P., Heat and Mass Transfer in a Saturated Porous Medium with Applications to Geothermal Reservoirs, Ph. D. Thesis, Mechanical Engineering Department, University of Colorado, Boulder, 294, 1978.

17. Goyal, K. P. and D. R. Kassoy, "A Plausible Two Dimensional Vertical Model of the East Mesa Geothermal Field, California U. S. A.," 1981 (to appear in J. of Geophys. Res.).

18. Sorey, M. L., Numerical Modeling of Liquid Geothermal Systems, Ph. D. Dissertation, University of California Berkeley, CA, p. 65, 1975.

19. Grindley, G. W., The Geology, Structure and Exploitation of the Wairakei Geothermal Field, Taupo, New Zealand, 131, 1965.

20. Grindley, G. W., Subsurface Structures and Relation to Steam Production in the Broadlands Geothermal Field, New Zealand, Geothermics: Proceedings of the United Nations Symposium on the Development and Utilization of Geothermal Resources, Vol. 2, part 1, special issue, 248-261, 1970.

21. Rinehart, C. D., and D. C. Ross, Geology and Mineral Deposits of the Mount Morrison Quadrangle, Sierra Nevada, California, U. S. Geological Survey, Professional Paper No. 385, 106, 1964.

22. Elders, W. A., R. W. Rex, T. Meidav, P. T. Robinson, and S. Biehler. Crustal Spreading in Southern California, Science, 178, 15-24, 1972.

23. Puente, C. I., and A. de la Peña, L., "Geology of the Cerro Prieto Geothermal Field," in the Proceedings of the First Symposium on the Cerro Prieto Geothermal Field, Baja California, Mexico, Lawrence Berkeley Laboratory, University of California, Berkeley, LBL-7098, 17-40, 1978.

24. Ward, P. L. and K. H. Jacobs, Microearthquakes in the Ahuachapan Geothermal Field, El Salvador, Central America, Science, 173, 328-330, 1971.

25. Combs, J. and D. Hadley, Microearthquake Investigation of the Mesa Geothermal Anomaly, Imperial Valley, California, Geophysics, 42(1), 17-33, 1977.

26. Bailey, T. P., A Hydrogeological and Subsurface Study of Imperial Valley Geothermal Anomalies, Imperial Valley, California, Geological Science, University of Colorado unpublished report, 101, 1977.

27. Riney, T. D., J. W. Pritchett, L. F. Rice and S. K. Garg, "Integrated Model of the Shallow and Deep Hydrothermal Systems in the East Mesa Area, Imperial Valley, California" SSS-R-79-3995, Systems, Science and Software, P.O. Box 1620, La Jolla, California 92038, p. 59, April 1979.

28. Riney, T. D. and J. W. Pritchett, "Integrated Model of the Shallow and Deep Hydrothermal Systems in the East Mesa Area, Imperial Valley, California" SSS-R-80-4215, Systems, Science and Software, P.O. Box 1620, La Jolla, California 92038, p 32, October 1979.

29. Goyal, K. P. and T. N. Narasimhan, "Constant Pressure Charging of a Liquid Dominated Geothermal Reservoir," Lawrence Berkeley Laboratory, University of California, Berkeley, LBL-11836, 1981.

Table 1.

d	P_b	R	τ	y_e
0.32	0.5	500	1	0.025
0.41	1	500	1	0.025
0.49	1.5	500	1	0.025
0.56	2	500	1	0.025
0.255	1	250	1	0.025
0.53	1	750	1	0.025
0.64	1	1000	1	0.025
0.96	1	500	1	0.05
0.41	1	500	2	0.025

FIGURE CAPTIONS

Fig. 1. Two-dimensional conceptual model of a liquid dominated geothermal reservoir.

Fig. 2. Temperature-depth profile for East Mesa wells below 800 meter depths (from Goyal and Kassoy [17]).

Fig. 3. Five different regions in the aquifer.

Fig. 4. Vertical velocity distributions along the depth of the fault for various values of P_b.

Fig. 5. Fault overpressures versus depth for various values of P_b.

Fig. 6. Nondimensional horizontal liquid velocity in the aquifer along the depth of the reservoir for different values of P_b.

Fig. 7. Fluid temperatures in the fault for various values of P_b.

Fig. 8. Fluid temperatures in the near fault regions 1 and 3 of the aquifer.

Fig. 9. Aquifer temperatures in the region 5.

Fig. 10. Surface temperature gradients along the length of the aquifer for different values of P_b.

Fig. 11. A comparison between the plots of M versus d and P_b versus d. (The data of M versus d from Goyal and Kassoy [9]).

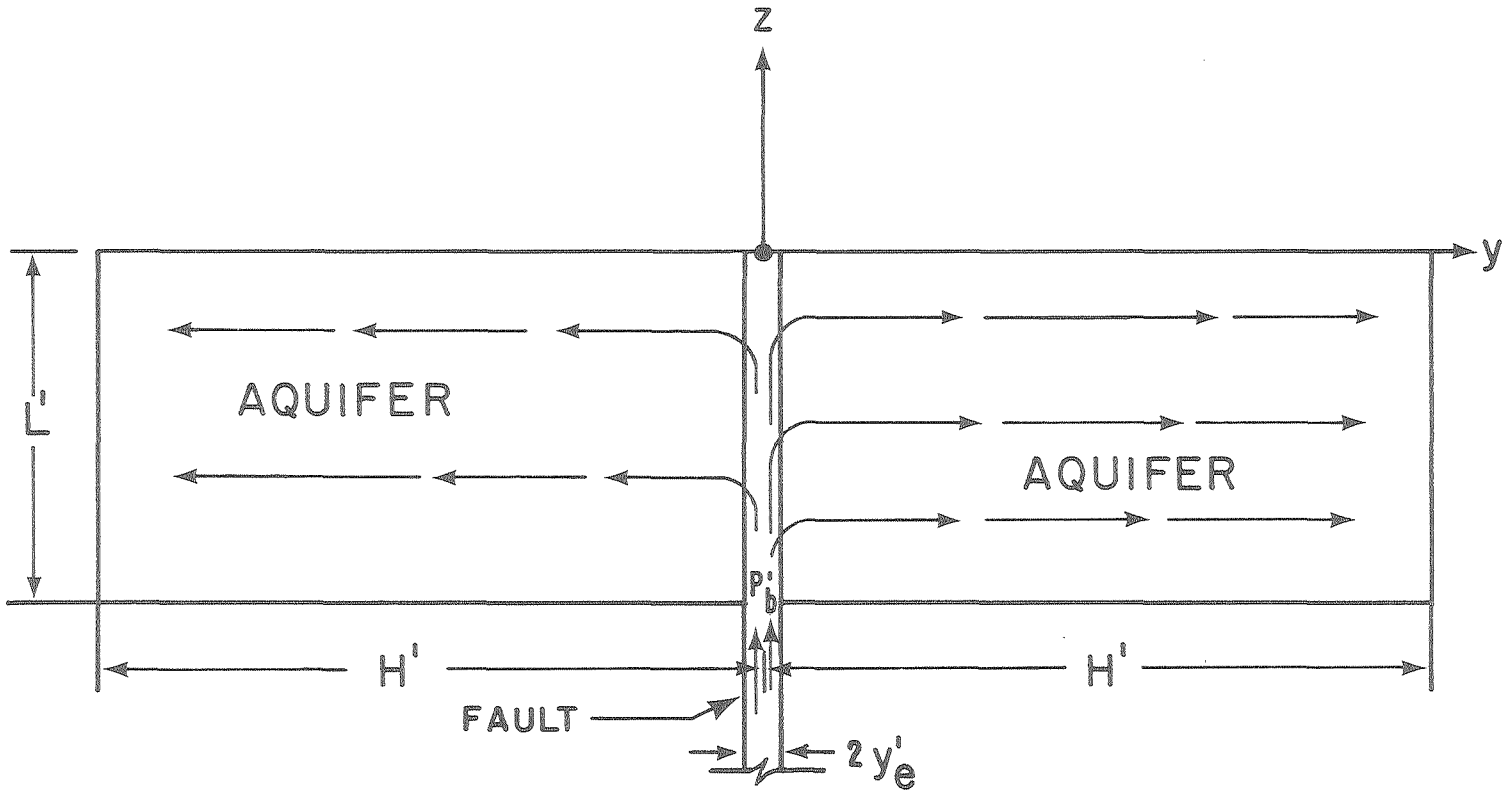

XBL 7812-2200A

Fig. 1. Two-dimensional conceptual model of a liquid dominated geothermal reservoir.

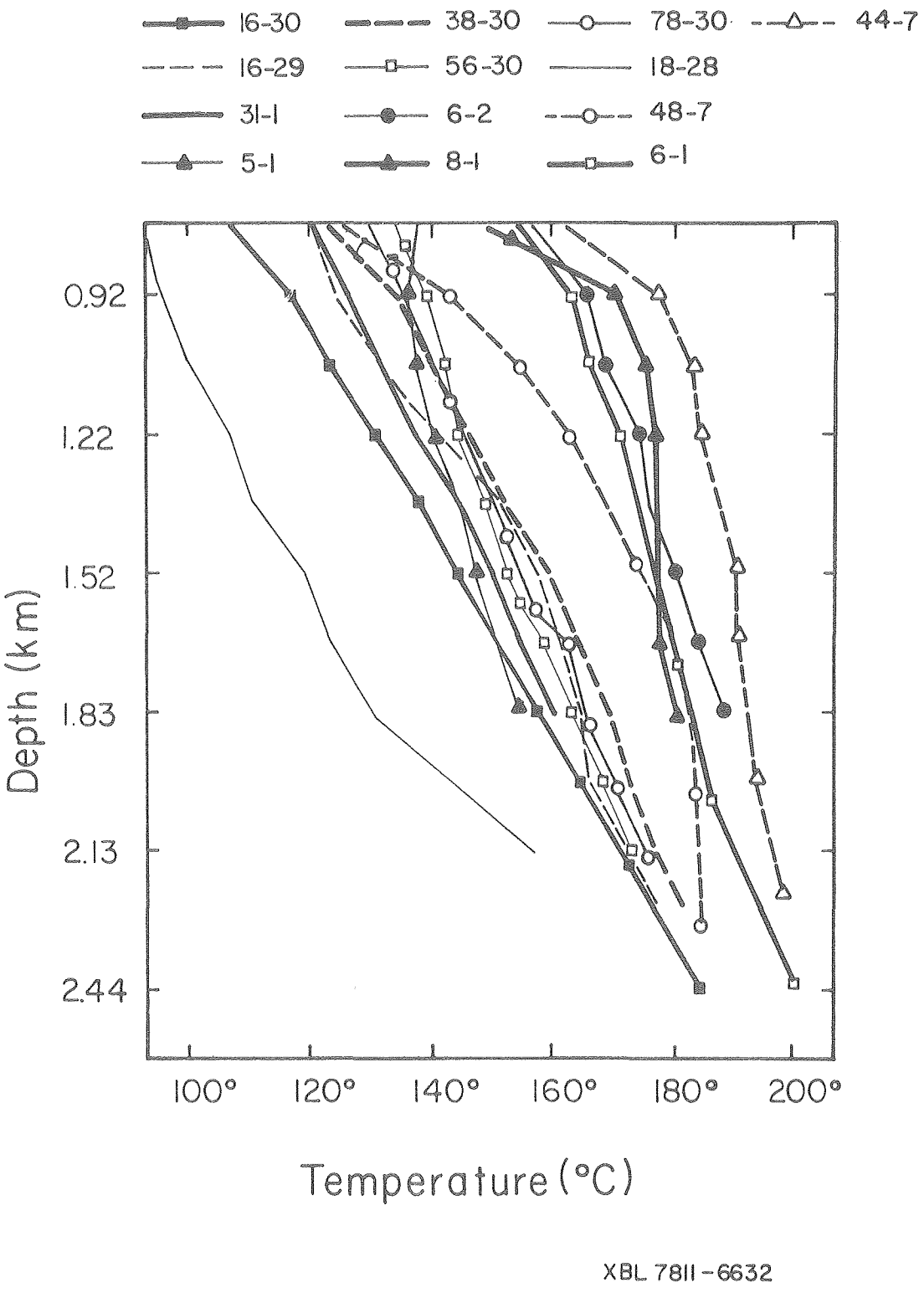

Fig. 2. Temperature-depth profile for East Mesa Wells below 800 meters depth (from Goyal and Kassoy [17]).

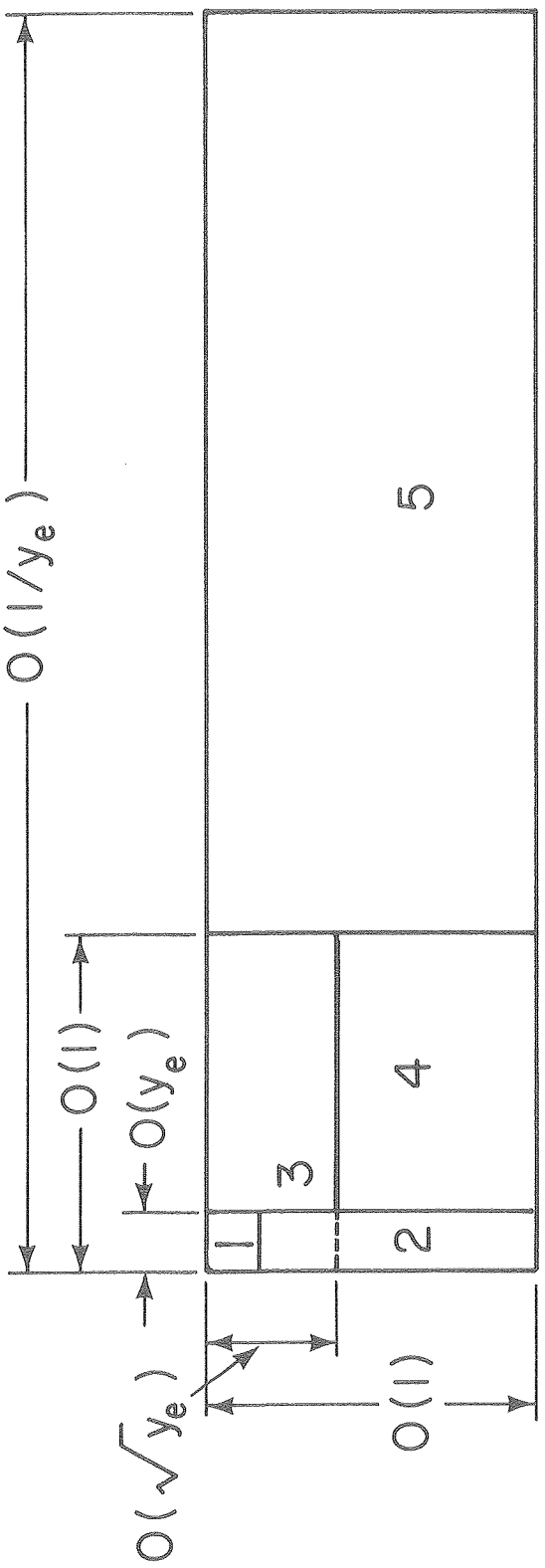

XBL 796-1978

Fig. 3. Five different regions in the aquifer.

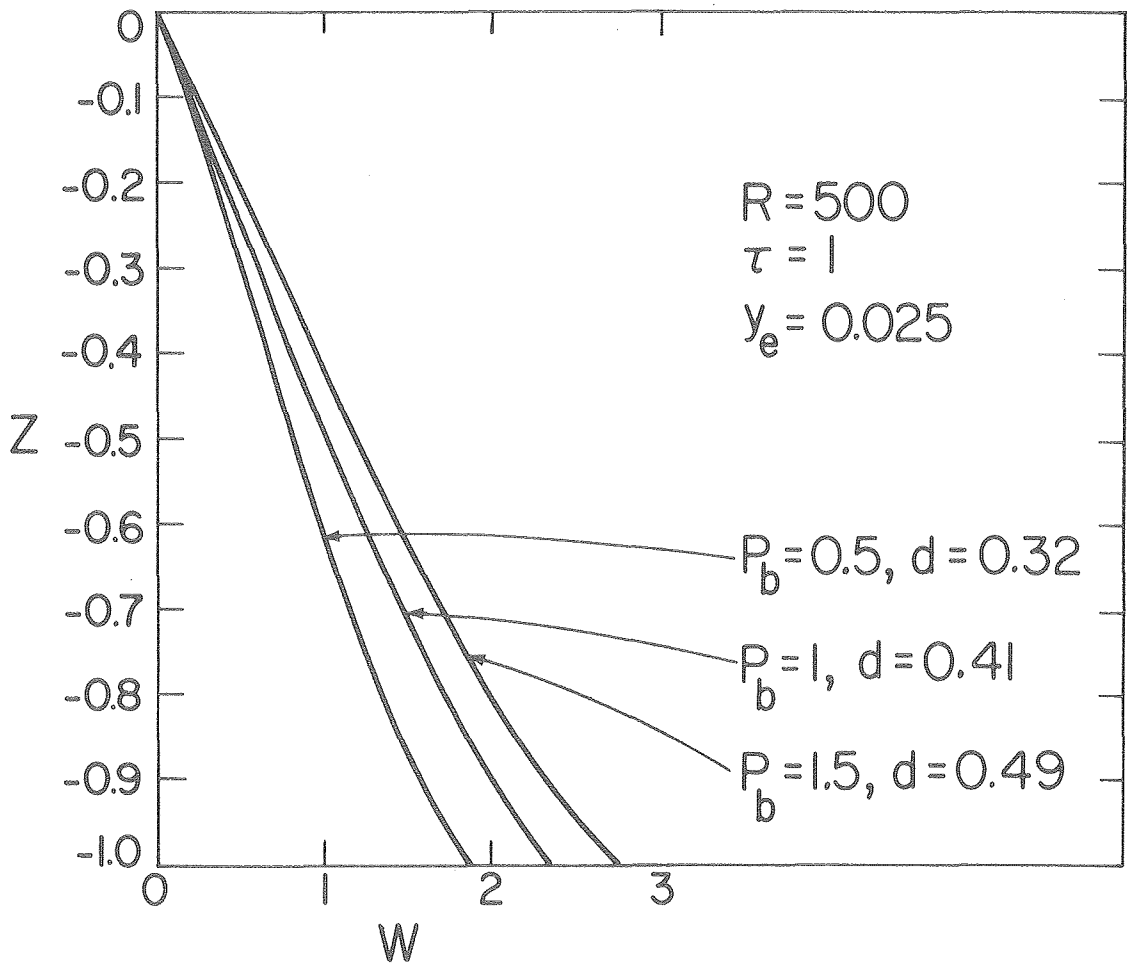

XBL 8011-2369

Fig. 4. Vertical velocity distributions along the depth of the fault for various values of P_b.

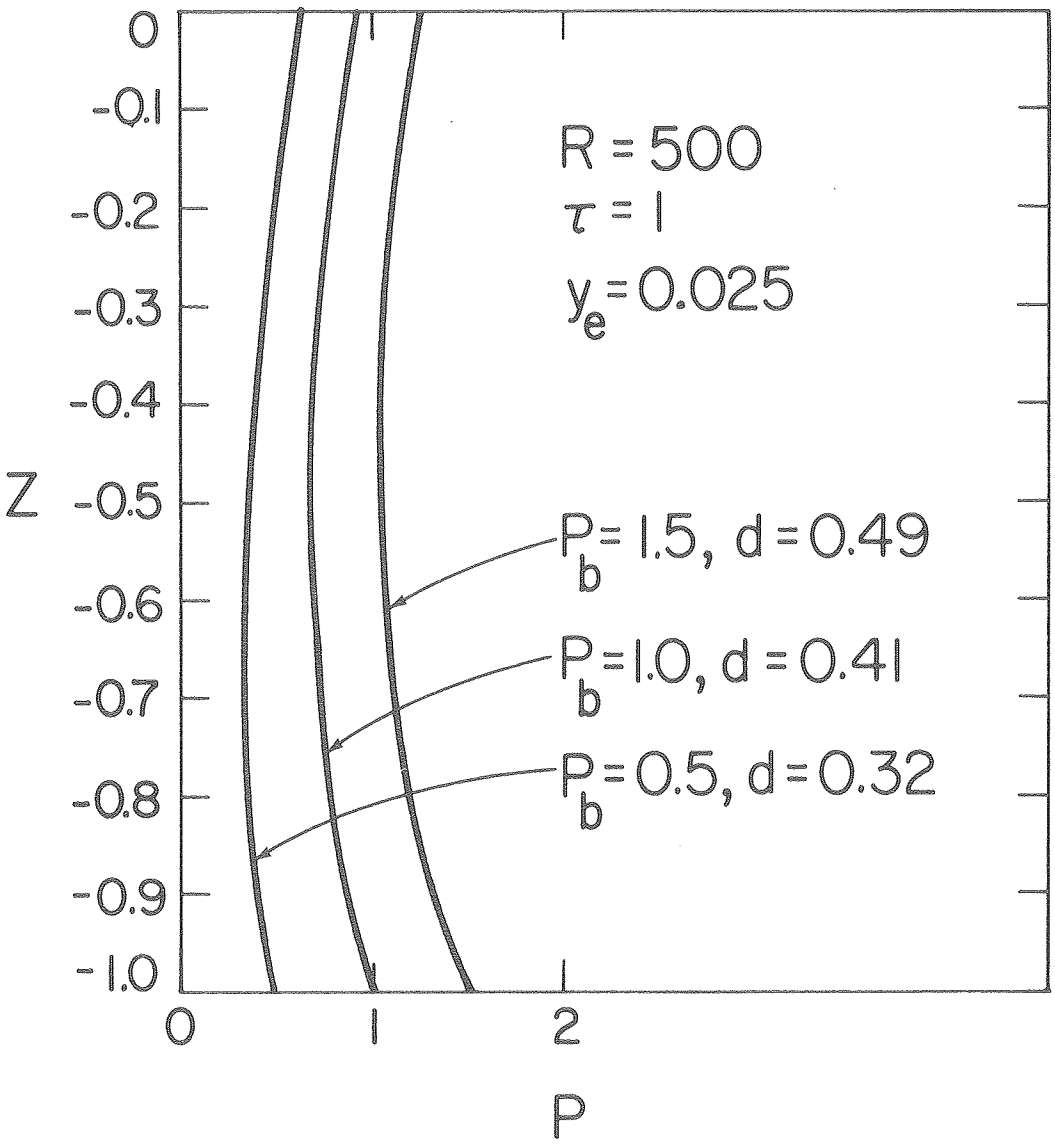

XBL 8011-2370

Fig. 5. Fault overpressures versus depth for various values of P_b.

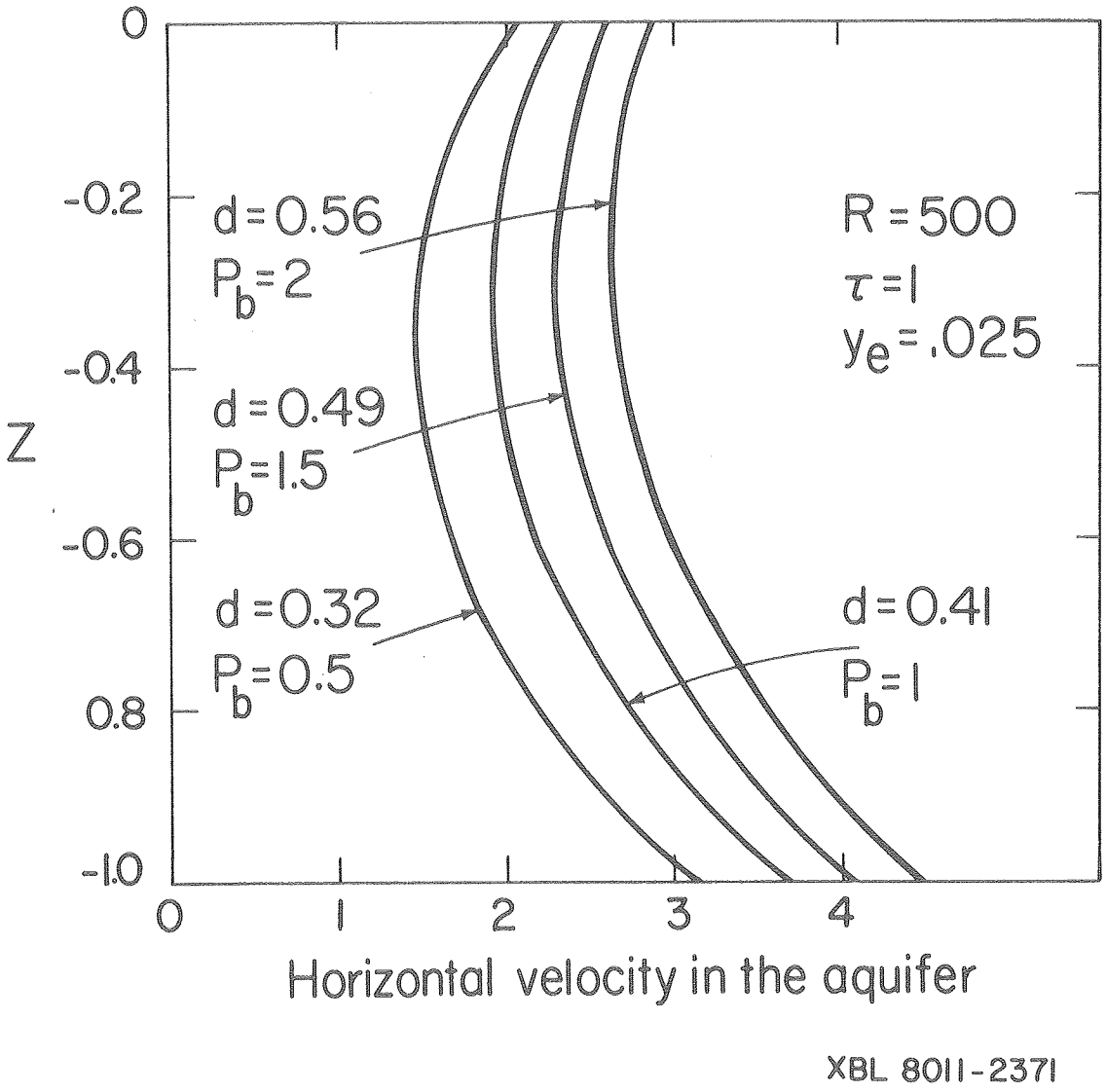

Fig. 6. Nondimensional horizontal liquid velocity in the aquifer along the depth of the reservoir for different values of P_b.

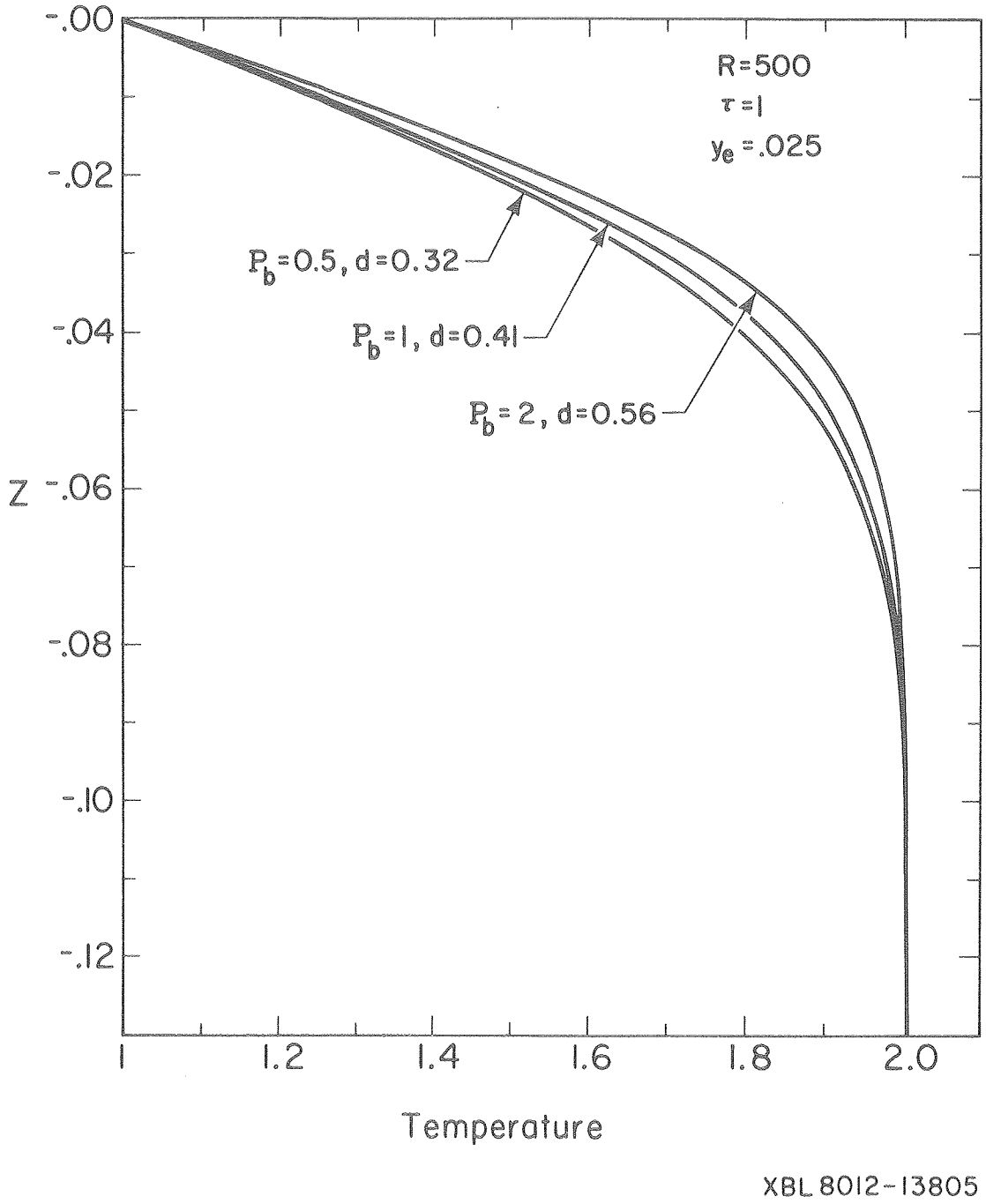

Fig. 7. Fluid temperatures in the fault for various values of P_b.

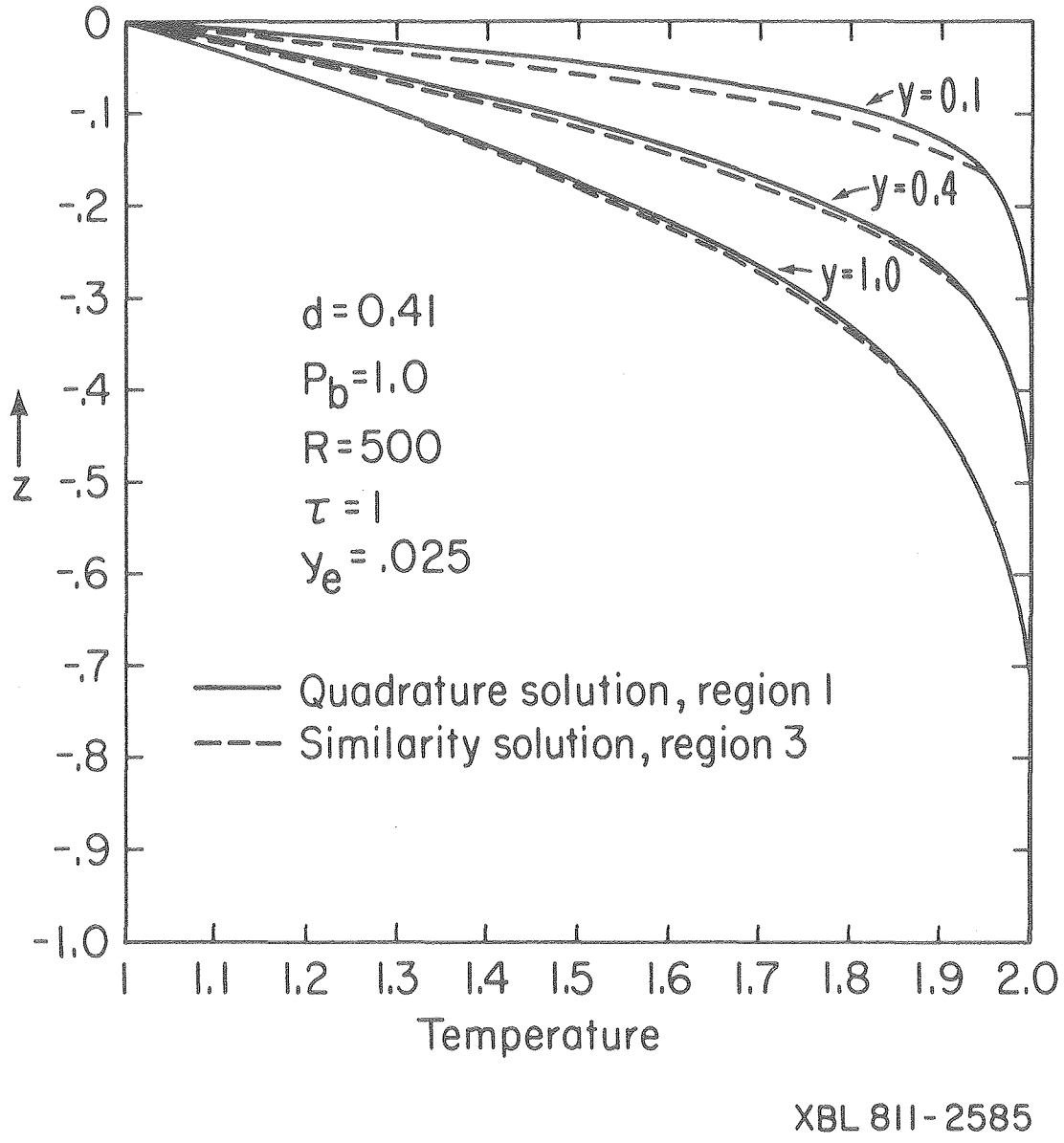

Fig. 8. Fluid temperatures in the near fault regions 1 and 3 of the aquifer.

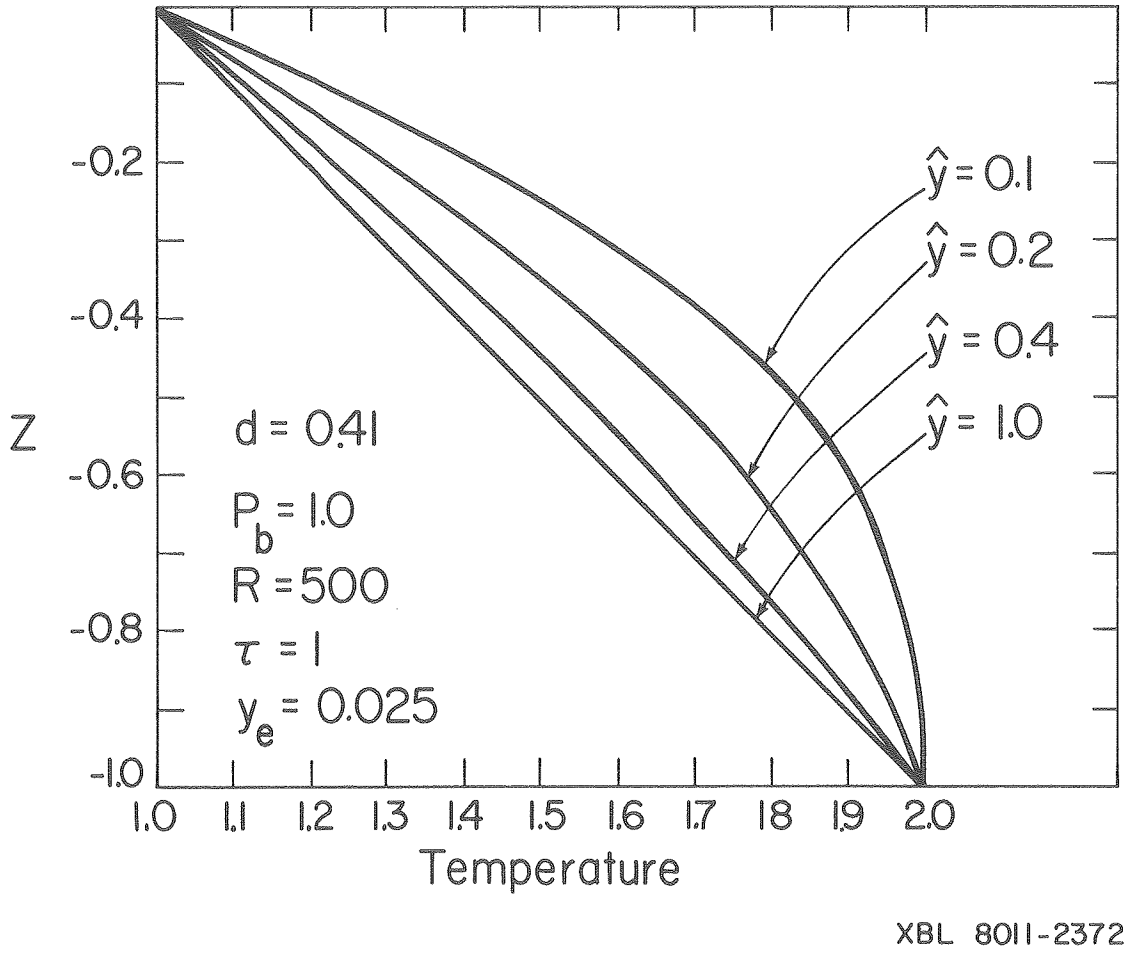

Fig. 9. Aquifer temperatures in the region 5.

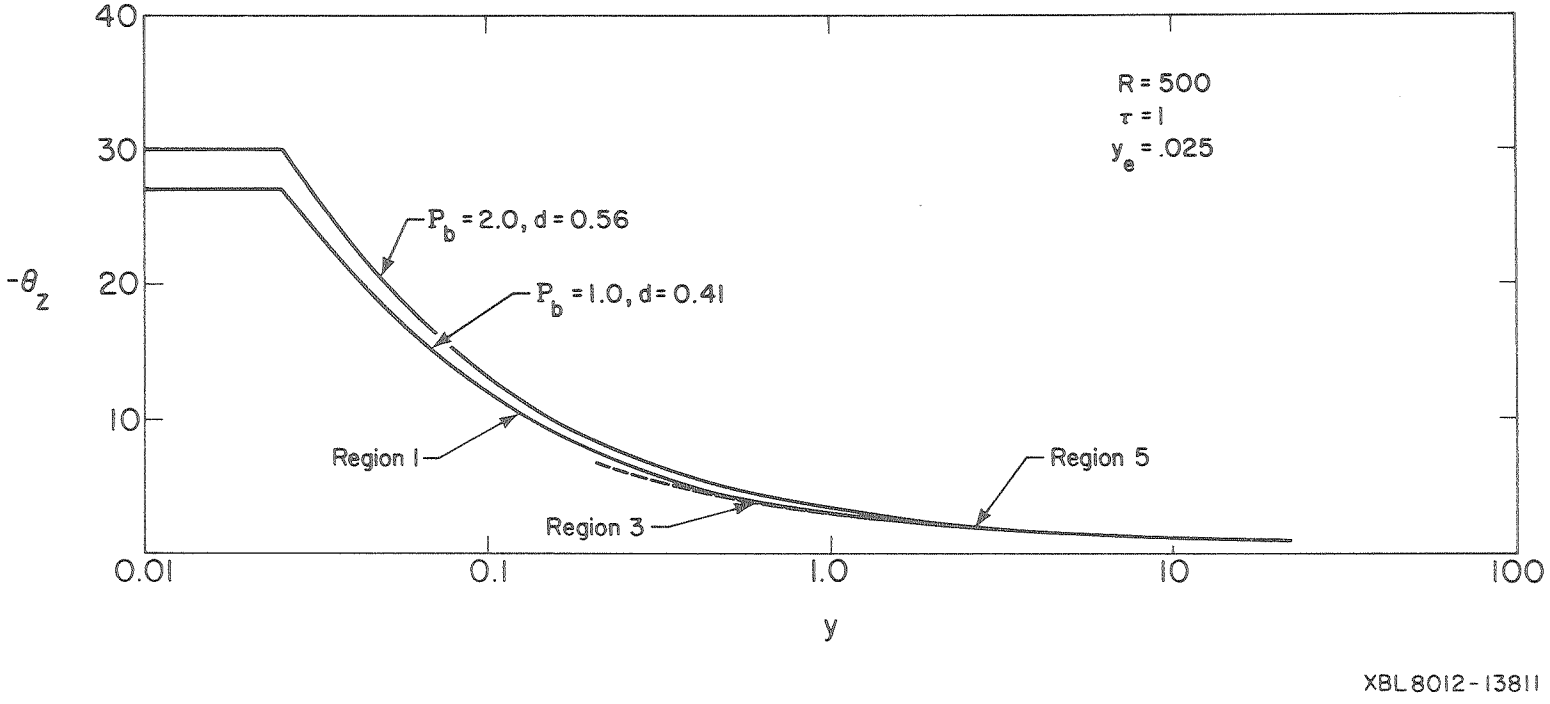

Fig. 10. Surface temperature gradients along the length of the aquifer for different values of P_b.

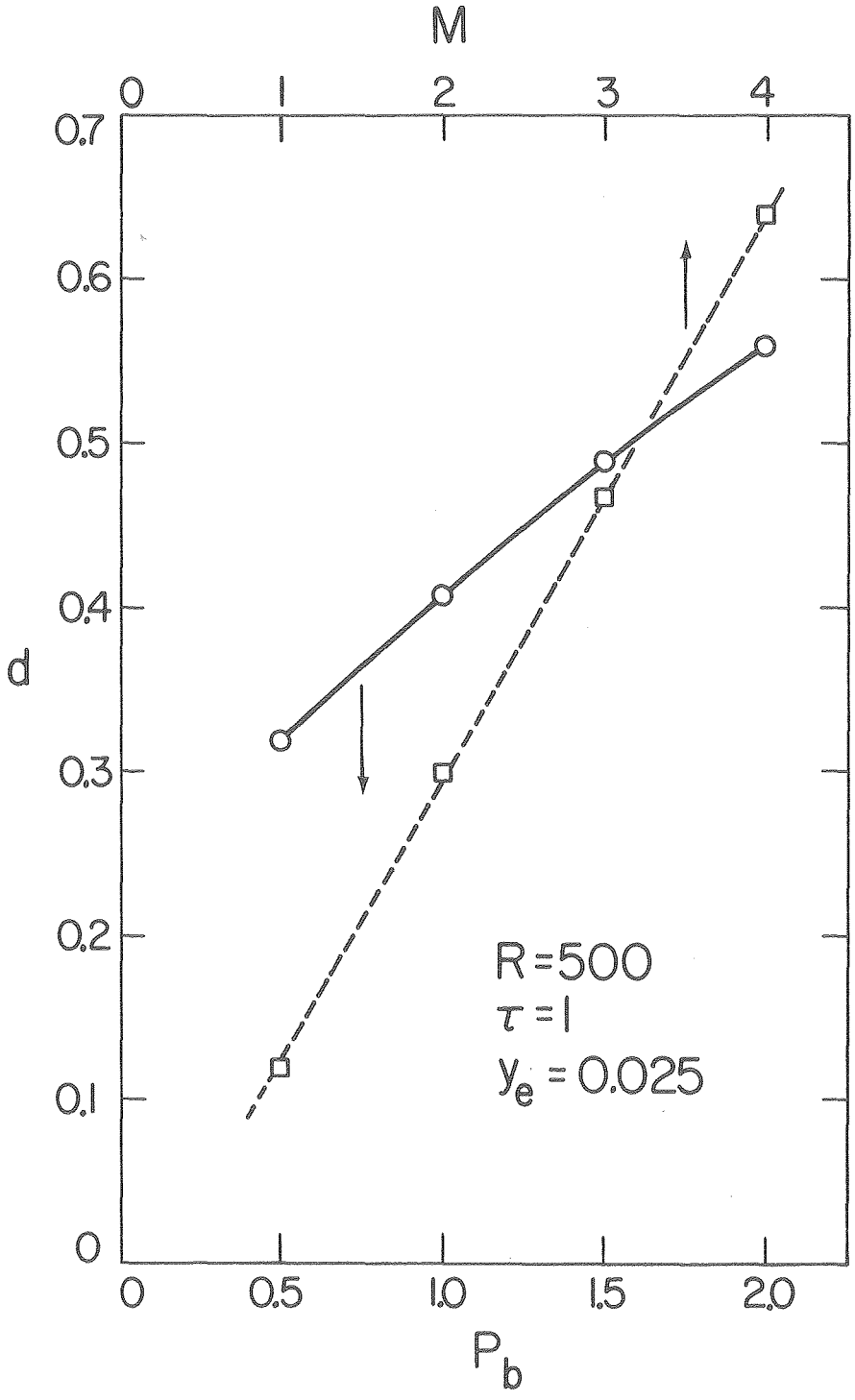

Fig. 11. A comparison between the plots of M versus d and P_b versus d. (The data of M versus d from Goyal and Kassoy [9]).